# Spin-Orbit Echo

N. Sugimoto and N. Nagaosa

*Science* **336**, 1413 (2012);
DOI: 10.1126/science.1217346

7. F. J. Fortea Pérez, *Bull. Soc. Préhistorique Ariège Pyrénées* **LVII**, 7 (2002).
8. A. W. G. Pike *et al.*, *J. Archaeol. Sci.* **32**, 1649 (2005).
9. D. L. Hoffmann, *Int. J. Mass Spectrom.* **275**, 75 (2008).
10. D. L. Hoffmann *et al.*, *Int. J. Mass Spectrom.* **264**, 97 (2007).
11. Materials and methods are available as supplementary materials on *Science* Online.
12. P. J. Reimer *et al.*, *Radiocarbon* **51**, 1111 (2009).
13. J. Zilhão, *Pyrenae* **37**, 7 (2006).
14. J. Zilhão *et al.*, *PLoS ONE* **5**, e8880 (2010).
15. J. Maroto *et al.*, *Quat. Int.* **247**, 15 (2012).
16. L. G. Straus, *Evol. Anthropol.* **14**, 145 (2005).
17. J. Zilhão, T. Aubry, F. Almeida, in *Les faciès leptolithiques du nord-ouest méditerranéen: milieux naturels et culturels. XXIV^e Congrès Préhistorique de France. Carcassonne, 26-30 Septembre 1994*, D. Sacchi, Ed. (Société Préhistorique Française, Paris, 1999), pp. 165–183.
18. C. Renard, *World Archaeol.* **43**, 726 (2011).
19. I. J. Fairchild, S. Frisia, A. Borsato, A. F. Tooth, in *Geochemical Sediments and Landscapes*, D. J. Nash, S. J. McLaren, Eds. (Blackwell, Oxford, 2007), pp. 200–245.
20. A. Beltran, *The Cave of Altamira* (Harry Abrams, New York, 1999)
21. C. González-Sainz, R. Cacho Toca, R. Fukazawa, *Arte Paleolítico en la Región Cantábrica* (Universidad de Cantabria, Cantabria, Spain, 2003).
22. F. Bernaldo de Quirós, *Proc. Prehistoric Soc.* **57**, 81 (1991).
23. C. Heras Martín, R. Montes Barquín, J. A. Lasheras, P. Rasines, P. Fatás Monforte, *Cuadernos de Arte Rupestre de Moratalla* **4**, 117 (2008).
24. H. Breuil, E. Cartailhac, H. Obermaier, M. E. Boyle, *The Cave of Altamira at Santillana del Mar, Spain* (Tip. de Archivos, Madrid, 1935).
25. H. Breuil, *Quatre cents siècles d'art pariétal. Les cavernes ornées de l'age du renne* (Centre d'Etudes de Documentation Préhistoriques, Montignac, Paris, 1952).
26. M. Lorblanchet, *Les Grottes Ornées de la Préhistoire. Nouveaux Regards* (Editions Errance, Paris, 1995).
27. F. Djindjian, in *Art Mobilier Paléolithique Supérieur en Europe Occidental*, A-C. Welté, E. Ladier, Eds. [Actes du Colloque 8.3, Congrès de l'UISPP (Union Internationale des Sciences Préhistoriques et Protohistoriques), Université de Liège, Liège, Belgium, 2004], pp. 249–256.
28. J. Clottes, J. Courtin, *The Cave Beneath the Sea: Palaeolithic Images at Cosquer* (H. N. Adams, New York, 2006).
29. R. de Balbín, J. J. Alcolea, M. A. González, in *El Arte Prehistórico Desde Los Inicios del s. XXI. Primer Symposium Internacional de Arte Prehistórico de Ribadesella*, R. de Balbín, P. Bueno, Eds. (Asociación Cultural de Amigos de Ribadesella, Ribadesella, Spain, 2003).
30. J. Clottes, *Return to Chauvet Cave: Excavating the Birthplace of Art* (Thames & Hudson, London, 2003).
31. P. B. Pettitt, P. Bahn, C. Züchner, in *An Enquiring Mind: Studies in Honor of Alexander Marshack*, P. Bahn, Ed. (American School of Prehistoric Research Monograph Series, Oxbow Books, Oxford, UK, 2009), pp. 239–262.
32. A. Broglio, M. de Stefani, F. Gurioli, M. Peresani, *Int. Newsl. Rock Art* **44**, 1 (2006).
33. B. Delluc, G. Delluc, *L'Art Pariétal Archaïque en Aquitaine* (Gallia Préhistoire XXVIII supplément, CNRS, Paris, 1991).
34. M. García-Diez, J. A. Mujika Alustiza, M. Sasieta, J. Arruabarrena, J. Alberdi, *Int. Newsl. Rock Art* **60**, 13 (2011).



**Acknowledgments:** This research was funded by a grant to A.W.G.P. from the Natural Environmental Research Council (NE/F000510/1). C. Taylor performed the sample preparation and assisted in collecting samples in the field along with C. Hinds, S. White, and S. Paine. We thank the governments of Asturias and Cantabria for granting permission to sample the cave art and B. Hanson for editorial guidance. The data described are presented in the supplementary materials.


**Supplementary Materials**

www.sciencemag.org/cgi/content/full/336/6087/1409/DC1
Materials and Methods
Figs. S1 to S12
Table S1
References (*35*–*39*)


1 February 2012; accepted 25 April 2012
10.1126/science.1219957




# Spin-Orbit Echo


**N. Sugimoto[1,2] and N. Nagaosa[1,2]***



**Preserving and controlling the quantum information content of spins is a central challenge of spintronics. In solids, the relativistic spin-orbit interaction (SOI) leads to a finite spin lifetime. Here, we show that spin information is preserved by the hidden conserved "twisted spin" and survives elastic disorder scatterings. This twisted spin is an adiabatic invariant with respect to a slow change in the SOI. We predict an echo phenomenon, spin-orbit echo, which indicates the recovery of the spin moment when the SOI is tuned off adiabatically, even after spin relaxation has occurred; this is confirmed by numerical simulations. A concrete experiment in two-dimensional semiconductor quantum wells with Rashba-Dresselhaus SOI is proposed to verify our prediction.**


For the manipulation of spin and spin current by electric fields in spintronics, the relativistic spin-orbit interaction (SOI) is essential because it connects the orbital motion and the spin of an electron (*1*). This interaction, however, destroys the rotational symmetry in the spin space and the consequent spin conservation law. In the presence of the SOI, there are several mechanisms to relax the spins by changing their direction at and between impurity scatterings (Fig. 1A) (*2*–*8*); spins decay with a (phenomenological) spin lifetime $\tau_s$, which is typically on the order of (or less than) 1 ns [(Fig. 1B, (i) to (iv)]. This is a serious issue for applications because the transfer and storage of information for a long time/distance is a crucial requirement for device function.

It has long been recognized that the SOI is closely related to the parallel transport and rotating frame comoving with the electron in the context of Thomas precession (*9*). This naturally leads to the formulation of the SOI in terms of the SU(2) spin gauge field $\hat{A}_\mu$ ($\mu = t, x, y, z$) connecting the neighboring frames in the nonrelativistic approximations to the Dirac equation (*10*–*12*). Based on this idea, there have been many attempts to find a conserved quantity by generalizing the spin (*11*–*17*). It has been known (*11*, *12*, *18*) that the electronic spin is only covariantly conserved as $D_0 s_a + \boldsymbol{D}\cdot\boldsymbol{j}_a = 0$, a spin density $s_a$, and a spin current density $\boldsymbol{j}_a$ ($a = x, y, z$); i.e., the continuity equation where the usual derivative $\partial_\mu$ is replaced by the covariant derivative $D_\mu := (D_0, \mathbf{D})$ holds. This means that the conservation law is satisfied in the comoving spin frame with the electron's motion but not in the laboratory frame. In a notable recent advance related to this concept, experiments were performed in semiconductor quantum wells with Rashba ($\alpha$) and Dresselhaus ($\beta$) SOIs described by $H_{RD} = \frac{p^2}{2m} + \alpha(p_y\sigma_x - p_x\sigma_y) + \beta(p_x\sigma_x - p_y\sigma_y)$, where $H_{RD}$ is the Rashba-Dresselhaus Hamiltonian, $\boldsymbol{p}$ is the momentum, m is the mass of an electron, $\sigma$s are the Pauli matrices, and $\hbar = 1$. In this system, the lifetime of a Fourier component of the spin $S_{\boldsymbol{q}}$ for $\boldsymbol{q} = (2\sqrt{2}m\alpha, 2\sqrt{2}m\alpha)$ [persistent spin helix (PSH)] is observed to be enhanced when the condition $\alpha = \beta$ is satisfied (*19*, *20*). In this case, the SU(2) gauge field strength $\hat{F}_{\mu\nu} \propto (\alpha^2 - \beta^2)\sigma_z$ is zero; that is, the SOI vanishes in the rotated spin frame.

We explicitly construct a conserved twisted spin in a generic situation when the electric field is regarded as a background static field (Fig. 1A). Furthermore, we study the adiabatic invariance of this twisted spin and predict a phenomenon called the spin-orbit echo [Fig. 1B, (iv) to (vii)]. The twisted spin preserves the information on the spin, and as the SOI is switched off adiabatically, the spin is recovered to coincide with the conserved twisted spin.

We consider a noninteracting electron system whose Hamiltonian is given by (*10*–*12*)

$$H = \frac{1}{2m}\left(\boldsymbol{p} - \frac{e}{mc^2}\hat{\boldsymbol{A}}\right)^2 + V(\boldsymbol{x}) \qquad (1)$$

where $\hat{\boldsymbol{A}} = \sum_{i,a} A_i^a \mathbf{e}_i \sigma_a / 2$, where $A_i^a := \sum_{jl} \varepsilon^{ial} E^l$ describes the SOI, $\mathbf{e}_i$ is the unit vector, and $V(\boldsymbol{x})$ is a scalar potential that includes the periodic crystal potential and the disorder potential. Here, $-e$ represents the charge of an electron; $c$ is the velocity of


[1]Department of Applied Physics, University of Tokyo, Tokyo 113-8656, Japan. [2]Cross-Correlated Materials Research Group and Correlated Electron Research Group, RIKEN, Saitama 351-0198, Japan.

*To whom correspondence should be addressed. E-mail: nagaosa@ap.t.u-tokyo.ac.jp

light; $\varepsilon^{ial}$ denotes the totally antisymmetric tensor; and $E^l$ is an electric field. Note that this Hamiltonian describes the SOI quite generally. The periodic part of $V(\boldsymbol{x})$ leads to band formation, and multiband effects are fully taken into account. Therefore, the SOI for an effective low-energy Hamiltonian that cannot be necessarily expressed through $\hat{\boldsymbol{A}}$ can also be described by Eq. 1 in the multiband formulation.

The definition of the twisted spin density $s_a^t$ for the generic Hamiltonian in Eq. 1 is given in eq. S11 (*21*, *22*); for concreteness, we consider here the Rashba-Dresselhaus Hamiltonian

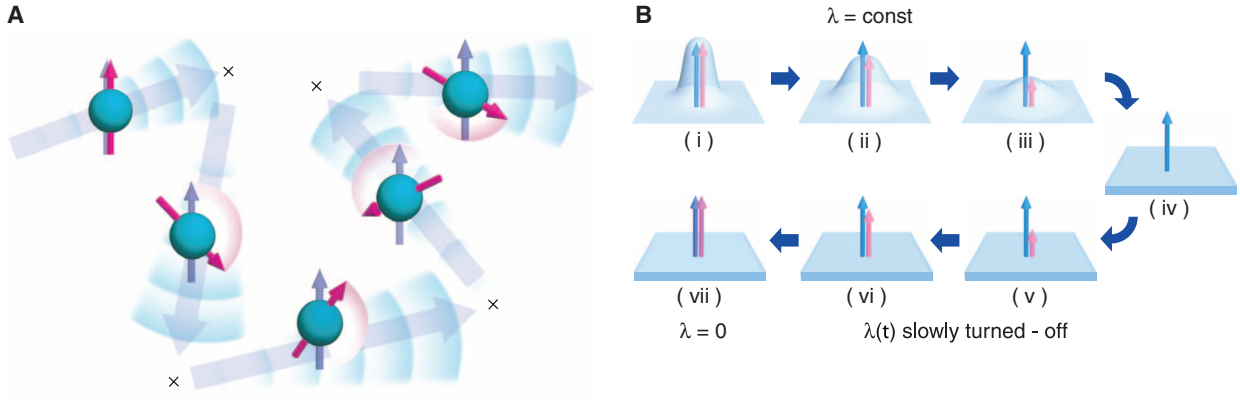


**Fig. 1.** (**A**) The electron spin (red arrows) changes its direction at and between scatterings by impurities (x symbols) in the presence of the SOI; the twisted spin (blue arrows) does not change. (**B**) Spin-orbit echo. Multiple impurity scatterings cause the diffusive motion of the electron, and the total spin (red arrows) decays in the presence of a constant SOI λ [stages (i) to (iv)]. As λ is reduced slowly to zero in (v) to (vii), the total spin is recovered and eventually coincides with the total twisted spin (blue arrows), which has remained constant during the whole process.

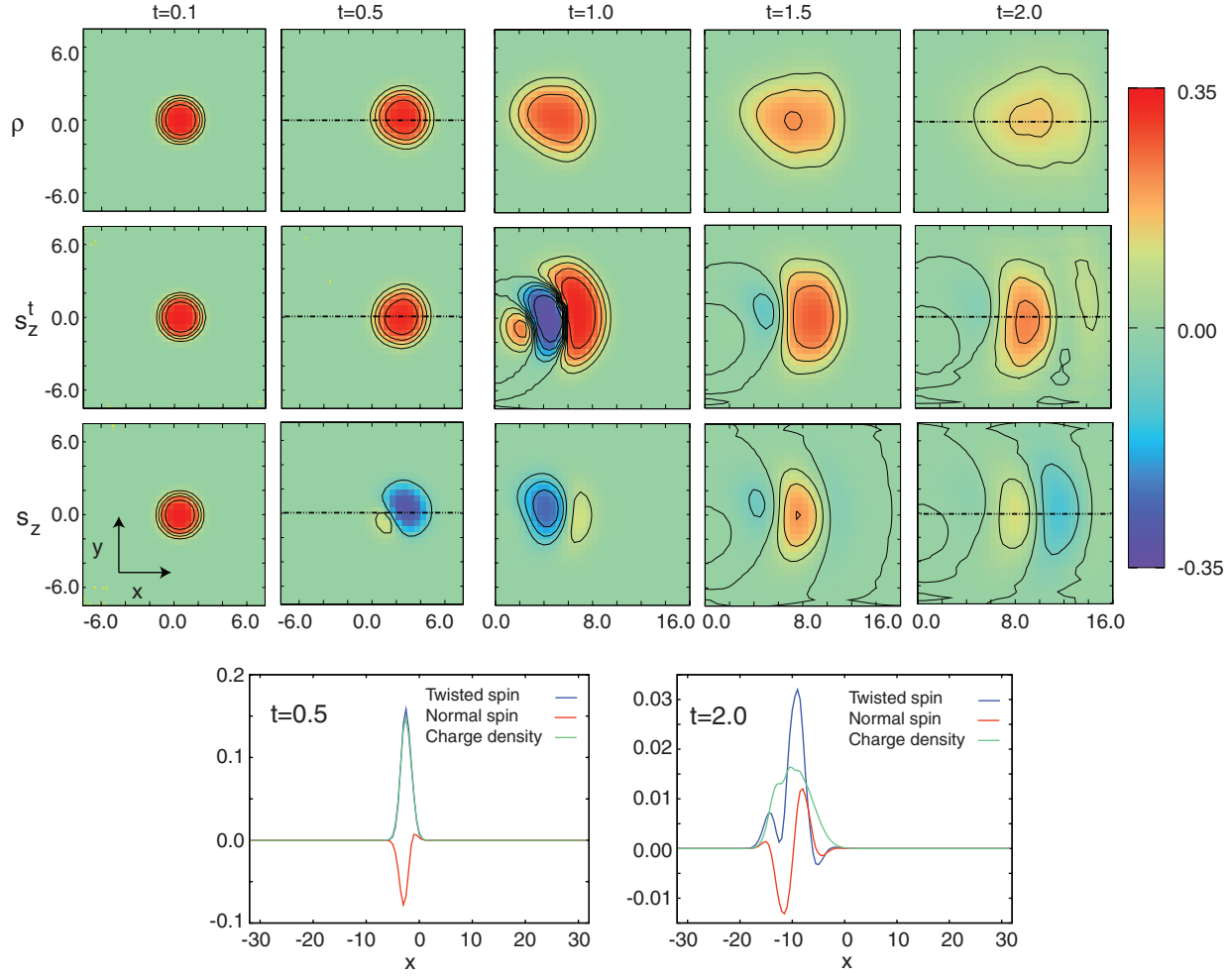


**Fig. 2.** Contour maps of charge density ρ (first row), twisted spin density $s_z^t$ (second row), and spin density $s_z$ (third row) at $t$ = 0.1, 0.5, 1.0, 1.5, and 2.0, where the Rashba SOI $\alpha$ = 0.8. The center of the initial wave function is at ($x$, $y$) = (0.0, 0.0) with the initial velocity ($v_x$, $v_y$) = (5.0, 0.0). The size of the sample is 64.0 by 16.0. The two bottom panels are the cross sections of the contour maps at $t$ = 0.5 and 2.0 along the dashed lines. ρ, $s_z^t$, and $s_z$ are shown in green, blue, and red, respectively.

$H_{RD}$. The twisted spin density is given by $s_a^t = \frac{\hbar}{2}\psi^\dagger Y^\dagger \sigma_a Y \psi$, where $\psi$ is the spinor, and the operator Y is given by

$$Y = \lim_{x' \to x} \frac{1}{2} e^{\frac{i}{2}m(\alpha+\beta)\sigma_- x_+} \times \left\{ e^{-\frac{i}{2}m(\alpha-\beta)\sigma_+ x_-} e^{-\frac{i}{2}\left[\overleftarrow{\partial}_x \frac{\sigma_z}{2m^2(\alpha^2-\beta^2)}\partial_y + \overleftarrow{\partial}_{y'} \frac{\sigma_z}{2m^2(\alpha^2-\beta^2)}\partial_x\right]} + e^{-\frac{i}{2}\left[\partial_{x'} \frac{\sigma_z}{2m^2(\alpha^2-\beta^2)}\partial_y + \partial_{y'} \frac{\sigma_z}{2m^2(\alpha^2-\beta^2)}\partial_x\right]} e^{-\frac{i}{2}m(\alpha-\beta)\sigma_+ x_-} + 2\sin^2\left[\frac{i(\partial_x - \partial_y)}{8\sqrt{2}m(\alpha+\beta)}\right] \right\} \quad (2)$$

with $\alpha > 0$ and $\beta > 0$. Here, $\sigma_\pm = \sigma_x \pm \sigma_y$, $x_\pm = x \pm y$, and $\overleftarrow{\partial}$ represents the differential operator acting only to the left. The usual conservation law $\partial_0 s_a^t + \nabla \cdot \boldsymbol{j}_a^t = 0$ is satisfied, where $\boldsymbol{j}_a^t$ is the twisted spin current density from eq. S11 (*21*, *22*). An important property of the twisted spin density is that it obeys the same transformation law as the usual spin density with respect to gauge transformation; by the SU(2) local gauge transformation $U_\alpha(\boldsymbol{x})$, the spinor, the gauge potential, and spin and twisted spin densities are transformed into $\chi'(\boldsymbol{x}) = U_\alpha(\boldsymbol{x})\chi(\boldsymbol{x})$, $\hat{A}'_\mu(\boldsymbol{x}) = U(\boldsymbol{x})\hat{A}_\mu(\boldsymbol{x})U^\dagger(\boldsymbol{x}) + U(\boldsymbol{x})\partial_\mu U^\dagger(\boldsymbol{x})$, $s'(\boldsymbol{x}) = R(\boldsymbol{x})s(\boldsymbol{x})$, and $(s^t)'(\boldsymbol{x}) = R(\boldsymbol{x})s^t(\boldsymbol{x})$, respectively. Here, $R(\boldsymbol{x})$ is an orthogonal 3-by-3 matrix; $U_\alpha^\dagger(\boldsymbol{x})\sigma_b U_\alpha(\boldsymbol{x}) = \sum_c R_{bc}(\boldsymbol{x})\sigma_c$. Note that Y is not a unitary operator for the SU(2) local gauge transformation, except for in the case of $\alpha = \beta$, because it includes a derivative operator. In the limit $\alpha \to \beta$, the factor $1/(\alpha^2 - \beta^2)$ in the exponent does not lead to a divergence because the $x'$ dependence vanishes in this limit, leading to a finite result as $Y \to U_\alpha = e^{im\alpha(\sigma_x - \sigma_y)(x+y)}$. The gauge potential is transformed into zero [i.e., $\hat{A}'_\mu(\boldsymbol{x}) = 0$], and $s_a^t$ becomes the persistent spin helix component $S_{\boldsymbol{q}}$ by this unitary transformation (*19*, *20*). Therefore, the twisted spin can be regarded as the generalization of the persistent spin helix.

From the continuity equation, the integral $S_a^t$ of the twisted spin density $s_a^t$ is constant; i.e., $dS_a^t/dt = 0$, even for the case of $\alpha \neq \beta$. The twisted spin conservation law can be regarded as the mapping of the covariant conservation law in the comoving frame to the laboratory frame for the generic case of nonzero $\hat{F}_{\mu\nu}$. The twisted spin conservation law means that some information related to spin is preserved, even after spin relaxation. We prove that $dS_a^t/dt$ does not contain terms linear in $d\lambda/dt$, where $\lambda$ is the SOI coupling constant (*21*, *22*); the leading order term is $\propto (d\lambda/dt)^2$ for a slow change in a spatially uniform $\lambda(t)$. Therefore, $S_a^t$ remains constant in the adiabatic limit $d\lambda/dt \to 0$, whereas the total change in $\lambda(t)$ is finite; $S_a^t$ is an adiabatic invariant. Therefore, the spin will be recovered completely when the SOI is switched off adiabatically within the inelastic lifetime—a phenomenon we term the spin-orbit echo. This is analogous to the spin echo in which the spin decaying within the elastic lifetime ($T_2$) can be recovered by a $\pi$-pulse within the inelastic lifetime ($T_1$).

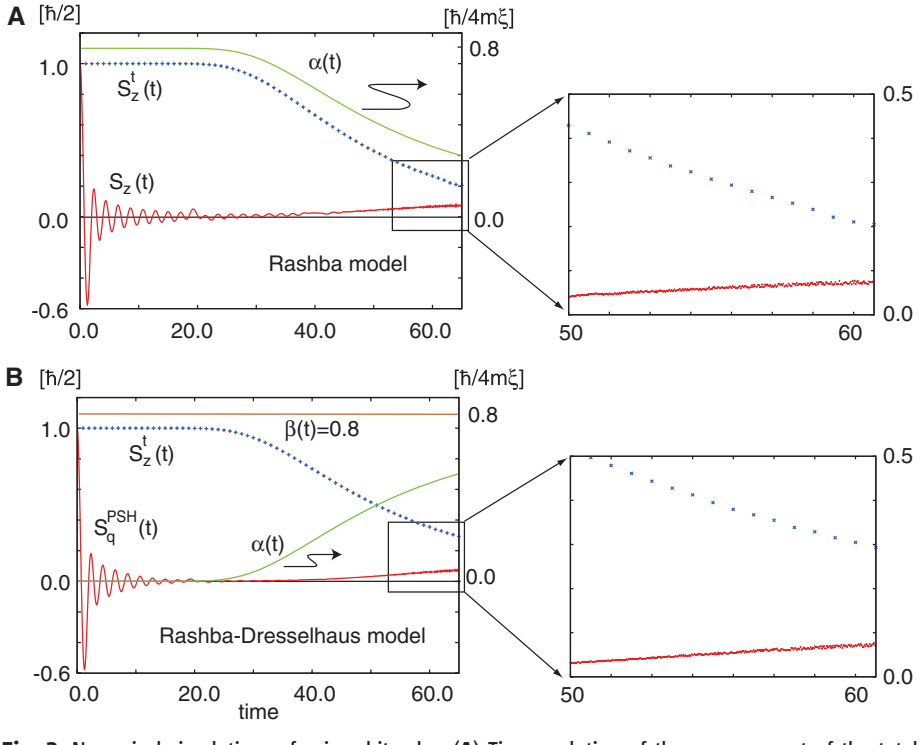


**Fig. 3.** Numerical simulations of spin-orbit echo. (**A**) Time evolution of the $z$ component of the total spin [$S_z(t)$, red curve] and total twisted spin [$S_z^t(t)$, blue dotted curve] for the Rashba SOI $\alpha(t) = 0.8 \times \tanh(\tau_\alpha^2/t^2)[\hbar/4m\xi]$ with $\tau_\alpha = 40$ (green curve) without the Dresselhaus SOI. (**B**) Spin-orbit echo of PHS $S_q^{PSH}$ in a Rashba-Dresselhaus system where the Rashba SOI varies as $\alpha(t) = 0.8 \times (1 - \tanh(\tau_\alpha^2/t^2))[\hbar/4m\xi]$ with $\tau_\alpha = 40$ ($t = 0 - 65$), and the Dresselhaus SOI $\beta = 0.8$ $[\hbar/4m\xi]$ is fixed.

The spin-orbit echo in disordered Rashba and Rashba-Dresselhaus models can be demonstrated by numerically solving the time-dependent Schrödinger equation for the Hamiltonian in Eq. 1 with a random potential $V(\boldsymbol{x})$ (*21*). The initial condition is taken to be a Gaussian wave packet $\psi(\boldsymbol{x}, t = 0) = \exp(-\boldsymbol{x}^2/2\xi^2 - im\boldsymbol{v}\cdot\boldsymbol{x})/\pi\xi^2$ with $\boldsymbol{v} = (5.0, 0.0)[1/m\xi]$, where the length unit is $2\xi$. The energy unit is $E_0 = 1/2m\xi^2$, the estimated kinetic energy of the initial wave packet for $\boldsymbol{v} = \boldsymbol{0}$. Figure 2 shows the time evolution of the charge wave packet, the $z$ component of spin ($s_z$), and twisted spin ($s_z^t$) densities for the Rashba model with $\alpha = 0.8[1/4m\xi]$. The center of mass of the charge density $\rho$ moves toward the right and in a downward direction corresponding to the anomalous Hall effect, whereas the positive and negative spin densities split, as in the spin Hall effect (*23*, *24*), and decay. In contrast, the twisted spin density $s_z^t$ is positive everywhere for $t \leq 0.5$, similar to the charge density (Fig. 2). For the period $0.5 < t \leq 2.0$, $s_z^t$ obtains some features of $s_z$ and eventually becomes spatially uniform.

Figure 3A shows the numerically obtained time evolution of the $z$ component of the total (integrated) spin $S_z(t)$ (red) and the total twisted spin $S_z^t(t)$ (blue) as $\alpha(t)$ is reduced according to $\alpha(t) = 0.8 \times \tanh(\tau_\alpha^2/t^2)[\hbar/4m\xi]$, with $\tau_\alpha = 40$ (green). $\beta = 0$ is fixed. The total spin $S_z(t)$ first relaxes in an oscillating fashion, whereas the total twisted spin $S_z^t(t)$ is conserved while $\alpha$ is constant. $S_z(t)$ recovers gradually from zero as the SOI is reduced, demonstrating the spin-orbit echo. Note that the recovery is not complete due to the finite rate of the decrease in $\alpha(t)$. This recovery will increase as the change in $\alpha(t)$ gets slower and slower and will eventually become perfect because $S_z^t$ is an adiabatic invariant.

In realistic cases, the Dresselhaus SOI still remains, even if the Rashba contribution can be tuned to zero. In this case, the SU(2) gauge invariant point $\alpha = \beta$ can be regarded to have no SOI in the rotated frame, and the total spin is interpreted as the PSH component $S_{\boldsymbol{q}}^{PSH}$. Figure 3B shows the time evolution of $S_{\boldsymbol{q}}^{PSH}$ as $\alpha(t)$ evolves from 0 to reach the SU(2) invariant point $\alpha(t = \infty) = \beta = 0.8[\hbar/4m\xi]$; i.e., $\alpha(t) = 0.8 \times [1 - \tanh(\tau_\alpha^2/t^2)][\hbar/4m\xi]$ with $\tau_\alpha = 40$. The recovery of $S_{\boldsymbol{q}}^{PSH}$ is seen as expected. Because the electric control of the Rashba SOI is established in GaAs quantum well systems (*25*), the spin-orbit echo is now realistic in the PSH system. In the experiment in (*25*), the Fermi wave number is $k_F \cong 10^8\ m^{-1}$, the momentum lifetime is $\tau/\hbar \cong 0.5 \times 10^5\ eV^{-1}$, and the spin splitting energy is $\Delta_\alpha \cong 10^{-3}$ eV. On the other hand, the parameters used in our simulations correspond to $k_F \cong 10^8\ m^{-1}$, $\tau/\hbar \cong 0.3 \times 10^4\ eV^{-1}$, $\Delta_\alpha \cong 2 \times 10^{-3}$ eV, and $t_{max} \sim 400$ ps.

In metals and semiconductors, four spin-relaxation mechanisms have been identified; the Elliott-Yafet (EY) (*2*, *3*), D'yakonov-Perel'(DP) (*4*, *5*), and Bir-Aronov-Pikus (BAP) (*6*) mechanisms, as well as hyperfine coupling with the nuclear spins. Inelastic scattering by phonons and electron/hole-electron interaction, such as the BAP mechanism, and magnetic scattering, such

as hyperfine interaction mechanism, will probably destroy the conservation of the twisted spin. However, the relevant inelastic lifetime increases as $\sim T^{-1}$ ($T$, temperature) and eventually becomes on the order of a nanosecond at $T \sim 0.1$ K (*26*, *27*); the BAP mechanism is absent in n-type materials. Additionally, the typical time scale of the spin lifetime resulting from hyperfine coupling is estimated at ~1 ns in n-type GaAs (i.e., longer than 400 ps). The cubic Dresselhaus SOI $\beta_3$ of $GaAs/Al_{0.3}Ga_{0.7}As$ quantum well samples is the dominant term causing the relaxation of the PSH, which is regarded as the nonpure gauge potential giving finite $\hat{F}_{\mu\nu}$, and gives the elastic EY and DP mechanisms (*20*). The enhanced spin lifetime on the order of 0.8 ns obtained in (*20*) is already long enough for the purpose of the spin-orbit echo discussed above. Therefore, it is anticipated that the spin-orbit echo can be tested at $T \sim 0.1$ K with the Rashba SOI tuned by electric field with the help of the optical grating method, as in (*20*).

### References and Notes


1. S. A. Wolf *et al.*, *Science* **294**, 1488 (2001).
2. R. J. Elliott, *Phys. Rev.* **96**, 266 (1954).
3. Y. Yafet, in *Solid State Physics*, F. Seitz, D. Turnbull, Eds. (Academic, New York, 1963), vol. 14, p. 2.
4. M. I. D'yakonov, V. I. Perel, *Sov. Phys. JETP* **33**, 1053 (1971).
5. M. I. D'yakonov, V. I. Perel, *Sov. Phys. Solid State* **13**, 3023 (1971).
6. G. L. Bir, A. G. Aronov, G. E. Pikus, *Sov. Phys. JETP* (Engl. transl.) **42**, 705 (1975) [transl. from *Zh. E'ksp. Teor. Fiz.* **69**, 1382 (1975)].
7. J. M. Kikkawa, D. D. Awschalom, *Phys. Rev. Lett.* **80**, 4313 (1998).
8. R. I. Dzhioev *et al.*, *Phys. Rev. B* **66**, 245204 (2002).
9. L. H. Thomas, *Nature* **117**, 514 (1926).
10. J. Fröhlich, U. M. Studer, *Rev. Mod. Phys.* **65**, 733 (1993).
11. P.-Q. Jin, Y.-Q. Li, F.-C. Zhang, *J. Phys. Math. Gen.* **39**, 7115 (2006).
12. B. W. A. Leurs, Z. Nazario, D. Santiago, J. Zaanen, *Ann. Phys.* **323**, 907 (2008).
13. T. W. Chen, C. M. Huang, G. Y. Guo, *Phys. Rev. B* **73**, 235309 (2006).
14. Y. Wang, K. Xia, Z. B. Su, Z. Ma, *Phys. Rev. Lett.* **96**, 066601 (2006).
15. R. Shen, Y. Chen, Z. D. Wang, D. Y. Xing, *Phys. Rev. B* **74**, 125313 (2006).
16. D. Culcer *et al.*, *Phys. Rev. Lett.* **93**, 046602 (2004).
17. J. Shi, P. Zhang, D. Xiao, Q. Niu, *Phys. Rev. Lett.* **96**, 076604 (2006).
18. C. N. Yang, R. L. Mills, *Phys. Rev.* **96**, 191 (1954).
19. B. A. Bernevig, J. Orenstein, S.-C. Zhang, *Phys. Rev. Lett.* **97**, 236601 (2006).
20. J. D. Koralek *et al.*, *Nature* **458**, 610 (2009).
21. For details, see the supplementary materials on *Science* Online.
22. N. Sugimoto, N. Nagaosa, http://arxiv.org/abs/1205.6629.
23. S. Murakami, N. Nagaosa, S.-C. Zhang, *Science* **301**, 1348 (2003).
24. J. Sinova *et al.*, *Phys. Rev. Lett.* **92**, 126603 (2004).
25. T. Koga, J. Nitta, T. Akazaki, H. Takayanagi, *Phys. Rev. Lett.* **89**, 046801 (2002).
26. B. J. F. Lin, M. A. Paalanen, A. C. Gossard, D. C. Tsui, *Phys. Rev. B* **29**, 927 (1984).
27. F. E. Meijer, A. Morpurgo, T. Klapwijk, T. Koga, J. Nitta, *Phys. Rev. B* **70**, 201307(R) (2004).



**Acknowledgments:** We thank K. Richter, V. Krueckl, and S. Onoda for fruitful discussion. This work is supported by Grant-in-Aid for Scientific Research from the Ministry of Education, Culture, Sports, Science and Technology of Japan; Strategic International Cooperative Program (Joint Research Type) from Japan Science and Technology Agency; and the Funding Program for World-Leading Innovative Research and Development on Science and Technology, Japan.


### Supplementary Materials

www.sciencemag.org/cgi/content/full/336/6087/1413/DC1
Supplementary Text
Fig. S1
References (*28*–*30*)


1 December 2011; accepted 27 April 2012
10.1126/science.1217346


# Dipolar Antiferromagnetism and Quantum Criticality in $LiErF_4$


**Conradin Kraemer,[1,2] Neda Nikseresht,[1] Julian O. Piatek,[1] Nikolay Tsyrulin,[1] Bastien Dalla Piazza,[1] Klaus Kiefer,[3] Bastian Klemke,[3] Thomas F. Rosenbaum,[4] Gabriel Aeppli,[5] Ché Gannarelli,[5] Karel Prokes,[3] Andrey Podlesnyak,[6] Thierry Strässle,[2] Lukas Keller,[2] Oksana Zaharko,[2] Karl W. Krämer,[7] Henrik M. Rønnow[1]***



Magnetism has been predicted to occur in systems in which dipolar interactions dominate exchange. We present neutron scattering, specific heat, and magnetic susceptibility data for $LiErF_4$, establishing it as a model dipolar-coupled antiferromagnet with planar spin-anisotropy and a quantum phase transition in applied field $H_{c\|} = 4.0 \pm 0.1$ kilo-oersteds. We discovered non–mean-field critical scaling for the classical phase transition at the antiferromagnetic transition temperature that is consistent with the two-dimensional XY/$h_4$ universality class; in accord with this, the quantum phase transition at $H_c$ exhibits three-dimensional classical behavior. The effective dimensional reduction may be a consequence of the intrinsic frustrated nature of the dipolar interaction, which strengthens the role of fluctuations.


The dipolar force between magnetic moments—a consequence of Maxwell's fundamental laws for electromagnetism—is present in all magnetic systems, from classical to quantum magnets, from bulk materials to nanoparticles. More than a half century ago, Luttinger and Tisza (*1*) discussed whether a polarized state of matter can be induced by classical dipole-dipole interactions alone and in the absence of short-range forces such as exchange interactions. They conjectured that both ferromagnetic (FM) and antiferromagnetic (AFM) order can arise, depending on the geometrical arrangement of the dipoles. When the modern theory of critical phenomena was developed, dipolar-coupled ferromagnets—in which the dipoles are atomic magnetic moments—presented material realizations on which concepts could be tested. Being three-dimensional (3D) systems, they were at the upper marginal dimension for the applicability of mean-field (MF) theory. This resulted in logarithmic corrections, which could be calculated exactly and agreed with the measured behavior around the classical phase transition (*2*). In the context of quantum phase transitions (QPTs), anisotropic dipolar systems are excellent realizations of, for example, the Ising model in a transverse field. In dipolar systems, the anisotropy ratio for the dipolar interaction scales as the square of the anisotropy ratio for response to an external magnetic field, and as a consequence, even for modest single-ion anisotropy the dipolar interaction along the hard axis is much smaller than along the easy axis. This hierarchy of scales is much harder to achieve in exchange-coupled systems in which the moment-carrying electron wave functions are responsible for both the exchange and single-ion anisotropies.

An excellent testing ground for the physics of dipolar-coupled systems are the lithium rare earth (*RE*) tetrafluorides, $LiREF_4$, in which tightly bound 4*f* electrons are far enough apart for the dipolar interactions to dominate exchange interactions. Another major advantage of the $LiREF_4$ family is the possibility of isostructural dilution with nonmagnetic yttrium, $LiRE_xY_{1-x}F_4$—permitting experiments from isolated dipoles (*3*) through disordered interacting dipoles forming spin glass states (*4*–*6*)—to the undiluted limit $LiREF_4$. To date, activity has centered on the Ising-like ferromagnets $LiTbF_4$ (*2*) and $LiHoF_4$ (*7*) and their respective dilution series (*8*). Here, we focus on an AFM member of the family $LiErF_4$ and address the magnetic order, the classical phase transition, and the transition and fluctuations about the quantum critical point.

Known as *RE*:YLF, very dilute ($x < 1\%$) $LiRE_xY_{1-x}F_4$ is used commercially in laser technology because of the long lifetimes of the crystal field energy levels of isolated $RE^{3+}$ ions. The crystal field also sets the stage for low-temperature collective properties. The electric field from neighboring ions act differently on the orbital wave-


[1]Laboratory for Quantum Magnetism, Ecole Polytechnique Fédérale de Lausanne (EPFL), 1015 Lausanne, Switzerland. [2]Laboratory for Neutron Scattering, Paul Scherrer Institute, 5232 Villigen, Switzerland. [3]Helmholtz-Zentrum Berlin, 14109 Berlin Wannsee, Germany. [4]James Franck Institute and Department of Physics, University of Chicago, Chicago, IL 60637, USA. [5]London Centre for Nanotechnology and Department of Physics and Astronomy, University College London, London WC1E 6BT, UK. [6]Oak Ridge National Laboratory, Spallation Neutron Source, Oak Ridge, TN 37831, USA. [7]Department of Chemistry and Biochemistry, University of Bern, 3000 Bern 9, Switzerland.

*To whom correspondence should be addressed; E-mail: henrik.ronnow@epfl.ch